

1. Publication Nº <i>INPE-3495-PRE/732</i>	2. Version	3. Date <i>April, 1985</i>	5. Distribution <input type="checkbox"/> Internal <input checked="" type="checkbox"/> External <input type="checkbox"/> Restricted
4. Origin <i>DMS/DCT</i>	Program <i>MATEDE/FISUP</i>		
6. Key words - selected by the author(s) <i>IMPURITY CLUSTERS DOPED SEMICONDUCTORS MANY-VALLEY EFFECTS</i>			
7. U.D.C.: <i>539.2</i>			
8. Title <i>SHALLOW IMPURITY CLUSTER STATES IN N-TYPE SEMICONDUCTORS</i>		<i>INPE-3495-PRE/732</i>	10. Nº of pages: <i>39</i>
			11. Last page: <i>38</i>
9. Authorship <i>A. Ferreira da Silva</i>			12. Revised by <i>Ram Kishore</i> Ram Kishore
Responsible author <i>A.F.S.</i>			13. Authorized by <i>MARCO ANTONIO RAPP</i> Marco Antonio Rapp Diretor Geral
14. Abstract/Notes  <i>Shallow impurity states are discussed for n-type semiconductors with emphasis on influence of the cluster states, type of disorder and many-valley character of the indirect-gap semiconductors. The random nature of the system is taken into account by analytical and simulation formalisms for the noninteracting one-band model and Hubbard and unrestricted Hartree-Fock-Roothaan models for correlated electrons. It is shown that in a wide range of impurity concentrations, such formalisms explain many of the electronic properties of doped semiconductors. The impurity states for a two-dimensional system are also discussed.</i>			
15. Remarks <i>Lecture presented at the II Escola Brasileira de Física de Semicondutores (II EBFS) - São Paulo, Feb. 4-15. To appear in the Special Issue of the II EBFS.</i>			

# SHALLOW IMPURITY CLUSTER STATES IN N-TYPE SEMICONDUCTORS

A. Ferreira da Silva

Instituto de Pesquisas Espaciais - INPE  
Conselho Nacional de Desenvolvimento Científico e Tecnológico - CNPq  
12200 São José dos Campos - SP - Brasil

## ABSTRACT

Shallow impurity states are discussed for n-type semiconductors with emphasis on influence of the cluster states, type of disorder and many-valley character of the indirect-gap semiconductors. The random nature of the system is taken into account by analytical and simulation formalisms for the noninteracting one-band model and Hubbard and unrestricted Hartree-Fock-Roothaan models for correlated electrons. It is shown that in a wide range of impurity concentrations, such formalisms explain many of the electronic properties of doped semiconductors. The impurity states for a two-dimensional system are also discussed.

## I. INTRODUCTION

In solid state physics we are familiar with the properties of crystalline materials (CM), in which electrons move in Bloch states extended throughout the whole material. The study of the electronic properties of such materials is simplified by the periodicity of the lattice which enables us to reduce the problem to the solutions of the Schrödinger equation in a single unit cell. Such a description of the electronic states of a crystalline material leads to a set of energy bands,  $\epsilon(k)$  -  $k$  being the crystal momentum, which extend to the surface of the Brillouin zone. In Fig. 1 we show schematically two distinct situations of a simplified bandstructure  $\epsilon(k)$ , and their corresponding density of states,  $D(\epsilon)$ . They are separated by an energy gap  $\Delta$  with a Fermi energy  $\epsilon_F$  indicating whether a band is partly or completely full. However, many important materials, such as alloys, liquids and amorphous solids, do not exhibit the strict periodicity of a crystal structure. Such materials, or the mathematical models used to describe them, have come to be classified under the general heading of disordered systems.

The first attempt to investigate, quantum mechanically, the electronic properties of a disordered system was made by Anderson.<sup>1</sup> He considered the motion of noninteracting electrons in a lattice of random potential wells, and formulated the problem within the tight binding approximation, given by the following Hamiltonian

$$H = \sum_i \epsilon_i a_i^\dagger a_i + \sum_{i \neq j} V_{ij} a_i^\dagger a_j, \quad (1)$$

where  $a_i^\dagger$  and  $a_i$  are, respectively, the creation and annihilation operators of an electron at the  $i$ -th site with energy  $\epsilon_i$ ; and  $V_{ij} (\equiv V(\vec{R}_{ij}))$  is the energy integral for the transfer of an electron from the  $i$ -th to the  $j$ -th site (hopping matrix elements). In this model, subsequently referred to as the Anderson model, the site energies are independent random variables, uniformly distributed with a width  $W$ , and the  $V_{ij}$  are taken as a constant  $V$  for nearest neighbours. Anderson has shown that such a model can support a new type of states, namely a

localized state, fundamentally different from extended Bloch states in respect of their transport properties. A localized state is what it implies, a state of the electron, localized in a finite region of space, with a wavefunction which, on the average, decays exponentially within this region. This is shown in Fig. 2. We find that, relative to the ordered system, illustrated by the sketch of the density of states in Fig. 1, the band is broadened, and the state in the tail up to energy  $\epsilon_C$  are of the localized type. At the energy  $\epsilon_C$ , known as mobility edge, the character of the states changes abruptly from localized to one which is essentially extended throughout the whole system. The position of  $\epsilon_F$  lying below  $\epsilon_C$  gives a metal-nonmetal (MNM) transition when it crosses  $\epsilon_C$ . Mott<sup>2</sup>, following Anderson's system, presented a clear exposition of the physics of MNM transition and suggested<sup>3</sup> that it might occur discontinuously. The electrical conductivity would jump from zero to a finite minimum value (minimum metallic conductivity) and then would increase smoothly at higher densities, in excellent agreement with many experiments.<sup>4</sup> On the other hand a scaling theory has been formulated which assumes that the MNM transition is continuous.<sup>5</sup> A much celebrated formula derived by Mott at which value would occur a MNM transition is  $N_C^{1/3} a_H^* \approx 0.25$ .<sup>2</sup> The formula was applied successfully to the MNM transition observed in doped semiconductor.<sup>6</sup> Here  $N_C$  is the impurity critical concentration and  $a_H^*$  is the effective Bohr radius of the donor electron.

The other theory was introduced by Hubbard<sup>7</sup> who used a tight binding model, in which the interaction between electrons is included only when they are on the same atom, long-range Coulomb forces being neglected. In the limit of infinite separation, the atomic limit, the ground state of a monovalent array of atoms is obviously a state in which each electron is bound to an atom. When an electron jumps to an occupied site, this means that electrical conduction requires an activation energy which is equal the repulsion energy  $U$  for two electrons occupying the same site. Thus for  $N$  atoms the energy spectrum consists of two separate sharp levels with  $N$ -fold degeneracy. The combination of such theories above consists in the well-known Mott-Hubbard-Anderson (MHA) model. An Hubbard Hamiltonian for disordered system is commonly written as<sup>7,8,9</sup>

$$H = \sum_{ij\sigma} V_{ij} a_{i\sigma}^{\dagger} a_{j\sigma} + \frac{1}{2} U \sum_{i\sigma} n_{i\sigma} n_{i-\sigma}, \quad (2)$$

where the first term was described above throughout Eq. (1), but now with spin  $\sigma$ , and  $V_{ij}$  playing the role of the random transfer integral; in the second term appears the interatomic Coulomb interaction (or correlation) energy  $U$  and the number operator  $n_{i\sigma} = a_{i\sigma}^{\dagger} a_{i\sigma}$ .

In the MHA model, the impurity density of states (IDS) is split into two Hubbard bands situated within the band gap of the host conduction band (HCB). When the impurity concentration is much less than  $N_c$ , these two IDS are identified as the lower ( $D^0$  - one electron per site) and upper ( $D^-$  - two electrons per site) Hubbard bands. With increasing impurity concentration, these bands will broaden and will eventually merge at  $N_c$ , see Fig. 3. The correlation effects is seen in the  $D^-$  state forming stable bound states, found experimentally by Narita and coworker<sup>10</sup> and investigated by Kamimura<sup>11</sup> in a many-valley semiconductor.<sup>12</sup> In essence, it appears that the role of the HCB in the phenomenon of MNM transitions is important primarily in the sense that it serves to determine the form of the cluster distribution of the (localized to extended) impurity states, as we will see later. In addition, recent work<sup>13</sup> has shown that the calculated value of the constant in Mott's condition  $N_c^{1/3} a_H^* = \text{const}$  is subject to the vagaries of the choice of electronic wave function, as well as being sensitive to the form of the HCB. The influence of the host characteristics, such as the existence of a conduction band with a many-valley character, is believed to be of central importance in the behavior of the physical properties and has been the subject of many recent investigations.<sup>13-20</sup> This inference does not apply to direct-gap semiconductors which have an isotropic conduction band (e.g., GaAs and CdS), and the isolated donor problem is thus just that of a hydrogen atom. On the other hand, in indirect-gap semiconductors (e.g., Si and Ge) the donor electron wave function is a sum over terms which are products of a rapidly oscillating Bloch wave with a hydrogenic envelope which satisfies an effective-mass Schrödinger equation. In silicon, there are six valleys in the HCB at  $\vec{k} \neq 0$ , and thus the 1s ground state of an isolated donor

has sixfold degeneracy in the framework of this effective-mass approximation, while germanium has four valleys.

The presence of different constitutional atoms<sup>21</sup> or the effect of a random field, as in the impurity band of a doped semiconductor, can be described in terms of random-mass in the site energies  $\epsilon_i$ . Within the context of the tight binding model, this is referred to as diagonal disorder.<sup>22</sup> Similarly, randomness in the off-diagonal matrix elements  $V_{ij}$  is called off-diagonal disorder. Clearly, in many cases, disorder of the diagonal and off-diagonal type will not be independent, but intimately linked. However, although interesting, such problems are mathematically highly complicated. Thus we expect that by studying the problem of diagonal and off-diagonal disorder by a computer cluster simulation through an unrestricted Hartree-Fock-Roothaan (HFA) scheme, we might gain information not only on their relevant systems, but also on their relative importance in a more complex structure. It is worth to mention that we also treat the problem of pure off-diagonal disorder analytically and by a cluster simulation in what follows.

## II. IMPURITY BAND MODEL

The model we use to discuss the IDS is the usual one, where we regard the extra charge on a donor impurity atom as forming a Coulomb centre on which the electron is bound with a hydrogen-like wavefunction. As an example we consider bulk Si for which the dielectric constant is 11.7 and the average effective mass is about 0.2 of the free electron value. Doping with P produces shallow impurity levels 0.045eV (0.61 Rydberg) below the HCB edge, and so we picture the electrons in hydrogen-like 1s state with a Bohr radius of the order of  $18\text{\AA}$ . Increasing doping the metallic state occurs at densities above  $N_C = 3.74 \times 10^{18} \text{cm}^{-3}$ . (At this point, the donors would be  $64\text{\AA}$  apart if they were ordered in a cubic lattice). For example, in Si:P the interelectron spacing =  $N_C^{-1/3} = 64\text{\AA}$ . Since the interatomic distance for Si is  $2.35\text{\AA}$ , we see that the orbit of the electron is sufficiently large that the lattice is very little distorted by the electron, which justifies the use of such a model. We can regard the impurities as completely randomly

distributed throughout the material, with only a restriction on the distance of closest approach of two impurities.

Matsubara and Toyozawa (MT)<sup>23</sup> developed an one impurity band approach, which treats the random distribution of the impurities by a Green's function expansion, but neglects electron and impurity correlations and the influence of the HCB. Their approach starts from an one-electron tight binding Hamiltonian

$$H = \epsilon_I \sum_i a_i^\dagger a_i + \sum_{i \neq j} V_{ij} a_i^\dagger a_j, \quad (3)$$

where the one-site energy  $\epsilon_I$  was assumed to be constant and taken as the negative value of the ionization energy of an isolated impurity and  $V_0 = 2\epsilon_I$  the unit for energy.

Using an one-band formalism, density of states have been obtained and compared with those of MT. Some improvements have been also carried out by the Heitler-London (HL)<sup>25</sup> and Alternant-Molecular-Orbital (AMO)<sup>26,27</sup> methods via hopping matrix elements  $V_{ij}$ , which show different behaviour for each method as presented in Fig. 4. As in MT the  $\epsilon_I$  is considered constant. It has been shown<sup>26,27</sup> that this assumption indeed holds for the impurity-concentration region of interest. See also Fig. 4. For the AMO calculation we show in Fig. 5 the IDS for different dimensionless impurity concentrations  $P = 32\pi N a_H^{*3}$ , where  $N$  is the true impurity concentration. In Fig. 6 we show the calculated impurity conductivity. Here, it is worth to mention that the impurity resistivities calculated by the present author did not take into account the many-valley character of the HCB<sup>27,28</sup> (e.g. for Ge and Si). As a first attempt if we divide them by the number of minima of the material we will get rough agreement with experiments<sup>26</sup>. Such study is object of our later work, as for example, following the idea of Saso<sup>29</sup>.

Another improvement of the model above is described by the Hubbard model, Eq. 2, in which calculations give the IDS<sup>8</sup> shown in Fig. 7. With decreasing impurity concentration Kamimura<sup>11,15</sup>, applying the MT

formalism to the MHA model, calculated the critical concentration  $p_c = 0.569$  with  $p_c = 32\pi N_c a_H^*{}^3$ , at which the IDS splits into two bands in agreement with the analytical determination of Kikuchi<sup>30</sup>. In the intermediate concentration region of impurity conduction, i.e., the transition region from insulating to metallic behavior, where the electron correlation plays an essential role, a characteristic activation energy  $\epsilon_2$  has been observed in the temperature and concentration dependences of the electrical conductivity<sup>31</sup>. These experimental observations have not been satisfactorily explained, but they suggest that in highly doped samples some delocalized conducting states are formed within the impurity states near the band edge of the HCB. This inference has been verified by far-infrared photoconductivity experiments<sup>32</sup>.

In Kikuchi's work, the energy gap between the Hubbard bands as a function of the impurity concentration has a remarkable similarity to the behavior of  $\epsilon_2$  for Ge:Sb. With increasing donor concentration from the low to high region, the  $\epsilon_2$  sharply decreases and vanishes at a critical concentration  $N_c$  where the MNM transition takes place.

Searching for a mechanism which enables us to take into account the degeneracy of the indirect-gap semiconductor, in the low to intermediate<sup>31</sup> n-type doping regime, i.e.,  $10^{16} \leq N < 2 \times 10^{17}$  and  $2 \times 10^{17} \leq N \leq 4 \times 10^{18} \text{cm}^{-3}$ , respectively, in Si:P and  $10^{15} < N \leq 10^{16}$  and  $10^{16} < N \leq 10^{17} \text{cm}^{-3}$  in Ge:Sb, we have performed an improvement in the IDS of our previous formalism (Refs. 8 and 22), with such degenerate effects. Considering the degeneracy of the HCB minima in Si and Ge via Fourier transform  $v(k)$  of  $V_{ij}$  we get the IDS for Ge:Sb and Si:P. They are shown in Fig. 8. In Figs. 9 and 10 we show the variation of the energy gap,  $\Delta g$ , between the IDS, compared to the experimental activation energy,  $\epsilon_2$ , of Ge:Sb and Si:P respectively.

### III. CLUSTER MODEL FOR IDS

Works to date have concentrated much effort in investigating cluster states which provide a great deal of interest in doped semiconductors,

particularly the Si:P system, which is a good system for, e.g., Raman studies, since it has the many-valley HCB necessary for a large electronic Raman cross-section,<sup>17</sup> as well as for electron spin resonance (ESR), photoconductivity, and far-infrared absorption spectra measurements, where cluster states have appeared in a dominant role. In the light of these investigations, some cluster approaches appeared in the literature, particularly those that take into account the many-valley character of the HCB. Franzén and Berggren,<sup>20</sup> using a Heisenberg Hamiltonian, calculated the magnetic susceptibility and specific heat in the low concentration region, well below  $N_c$ , found good agreement with experimental results in Si:P. For the exchange interaction, they used the Kohn-Luttinger (KL) (Ref. 33) wave functions because of the many-valley semiconductors in Si.

With a computer we generate  $M$  random impurity sites  $\{R_i; i = 1, M\}$  within a volume  $\Omega$  of a diamond lattice as a host, as the locations of  $M$  substitutional impurities, in order to simulate a sample of a doped semiconductor with impurity concentration  $N = M/\Omega$ . Surrounding these  $M$  impurities, another  $M_s$  impurities were similarly generated, in such a way as to keep the impurity concentration unchanged. These  $M_s$  impurities are included to reduce surface effects and provide a mean field. With each impurity of the inner  $M$  impurities embedded in this mean field is associated a KL donor wave function  $\psi_i$  given by

$$\psi_i(\vec{r}) = \frac{1}{\sqrt{\nu}} \sum_{\ell=1}^{\nu} F_{\ell}(\vec{r}) \phi_{\ell}(\vec{r}), \quad (4)$$

where  $\phi_{\ell}(\vec{r})$  is the Bloch function associated with the  $\ell$ th of the  $\nu$  conduction-band minima of the host material ( $\nu = 6$  for silicon), and  $F_{\ell}(\vec{r})$  is a hydrogenic envelope function in which the effective mass at each of these minima has been assumed to be isotropic. Thus the calculation is simplified, since the envelope function can be written as

$$F_{\rho}(\vec{r}) = (\pi/\alpha^3)^{1/3} \exp(-\alpha r) , \quad (5)$$

where  $\alpha = 1/a_H^*$ .

The Hamiltonian of the many-electron system is

$$H = \sum_i \frac{p_i^2}{2m} + \sum_i V^{\text{ion}}(\vec{r}_i) + \frac{1}{2} \sum_{i,j} V^{\text{el-el}}(\vec{r}_i - \vec{r}_j) , \quad (6)$$

where  $V^{\text{ion}}(\vec{r}_i)$  is the impurity-ion potential acting on the  $i$ th electron,  $V^{\text{el-el}}(\vec{r}_i - \vec{r}_j)$  is the Coulomb interaction between the  $i$ th and  $j$ th electron, and the summations are over all the  $M$  electrons in the volume  $\Omega$ . This inner cluster will be solved numerically using an unrestricted HFR formalism with spin-polarized potential. This formalism<sup>34</sup> turns out to be similar to the Hartree-Fock theory used in previous calculations.<sup>22</sup> Accordingly, the following two sets of coupled Schrodinger equations arise:

$$H_{\sigma}(\vec{r}) \psi_{n\sigma}(\vec{r}) = E_{n\sigma} \psi_{n\sigma}(\vec{r}), \quad \sigma = \uparrow, \downarrow \text{ and } n = 1, M \quad (7)$$

where

$$H_{\sigma}(\vec{r}) = \frac{p^2}{2m} + V^{\text{ion}}(\vec{r}) + V^{\text{C}}(\vec{r}) + V_{\sigma}^{\text{ex}}(\vec{r}) , \quad (8)$$

$V^{\text{C}}(\vec{r})$  is the Coulomb potential, and  $V_{\sigma}^{\text{ex}}(\vec{r})$  is the spin-dependent exchange potential.<sup>34</sup>

The eigenstates of Eq. (7) can be expressed as

$$\psi_{n\sigma}(\vec{r}) = \sum_j \psi_j(\vec{r}) B_{jn\sigma} , \quad (9)$$

where  $\psi_j(\vec{r})$  are given by Eq. (4).

Following the usual HFR procedure, we obtain

$$\sum_j [\bar{B}_\sigma^\dagger \bar{H}'_\sigma \bar{B}_\sigma]_{ij} - E_m \delta_{ij} ] C_{mj} = 0 , \quad (10)$$

where the matrix elements of  $\bar{H}'_\sigma$  are given by

$$\begin{aligned} H'_{ii\sigma} = & E_I + \alpha \sum_{k \neq i} J(\alpha \vec{R}_{ik}) + [UP_{ii}^{-\sigma} + 2 \sum_{k \neq i} P_{ij}^{-\sigma} L(\alpha \vec{R}_{ik}) \\ & + \sum_{s=\sigma, -\sigma} \sum_{k \neq i} P_{kk}^s J'(\alpha \vec{R}_{ik}) - \sum_{k \neq i} P_{kk}^\sigma K'(\alpha \vec{R}_{ik})] \alpha , \end{aligned} \quad (11)$$

$$\begin{aligned} H'_{ij\sigma} = & E_I S(\alpha \vec{R}_{ij}) + [K(\alpha \vec{R}_{ij}) + (P_{ii}^{-\sigma} + P_{jj}^{-\sigma}) L(\alpha \vec{R}_{ij}) \\ & + \sum_{s=\sigma, -\sigma} P_{ij}^s K'(\alpha \vec{R}_{ij}) - P_{ij}^\sigma J'(\alpha \vec{R}_{ij})] \alpha . \quad (E_I \equiv \epsilon_I) \end{aligned} \quad (12)$$

Some of these Slater integrals are multiplied by an interference factor, denoted here by  $I$ , derived from the many-valley character of the HCB, which is assumed as a valley-symmetric wave function. It is obtained as<sup>34,35</sup>

$$I = \frac{1}{v} \sum_{\ell=1}^v \exp(i \vec{k}_\ell \cdot \vec{R}) . \quad (13)$$

As a consequence of the valleys in Si, for instance, the overlap and the hopping integrals have an oscillatory behavior as shown in Fig. 11, which will reduce the broadening of the IDS. Neglecting the third and fourth terms in Eq. 8 the formalism reduces to an one-band model, compared to MT scheme.<sup>35</sup> In Fig. 12 we show the IDS for this latter model with and without many-valley character of the HCB, as well as the effect of nonorthogonality,<sup>22,36</sup> for  $P = 1$ , corresponding to  $N = 1.92 \times 10^{18} \text{cm}^{-3}$  in Si:P. The dots appearing on these figures are the inverse participation ratio (IPR) discussed below.

#### IV. IMPURITY CLUSTER STATES, IDS AND DISCUSSION

In Eqs. (11) and (12) we can vary  $\alpha$  in order to get the optimum value of  $\alpha$  which gives the two bands centered on their real values. Accordingly the center of gravity of  $D^0$  ( $\langle D^0 \rangle$ ) remains almost uncharged in  $-1.0$  Ry, while  $\langle D^- \rangle$  varies until we catch the optimum value of  $\alpha \approx 0.8$  which gives the experimental value  $10 \langle D^- \rangle = 0.0555$  Ry ( $-0.0275$  effective hartree). In Figs. 13 and 14 we show such a scheme.<sup>37</sup> We also use  $\alpha = 1$  and the corresponding experimental value  $U/V_0 = 0.475$  to calculate the IDS, - the term  $U$  remains unaltered at  $5/8$  (effective hartree) with the inclusion of many-valley effect. In this case, again the  $\langle D^0 \rangle$  remains unaltered while  $\langle D^- \rangle$ , at very low concentration, is lowered to a value of  $-0.0275$  effective hartree which is consistent with the value found above. Such value was also found by Riklund and Chao<sup>38</sup> in their HF IDS calculation using a Chandrasekhar wave function.

The IDS  $D(E)$  is normalized to

$$\int D(E) dE = \frac{p}{32\pi} = (M/\Omega) a_H^{*3}, \quad (14)$$

where  $p$  is defined as a dimensionless impurity concentration  $p = 32\pi M a_H^{*3} / \Omega$ . For Si:P the critical concentration is around  $p_c \approx 2.0$ , taking  $a_H^* = 17.3 \text{ \AA}^0$  and  $N_c = 3.74 \times 10^{18} \text{ cm}^{-3}$  (Ref. 4). In our calculation we use inner clusters of  $M = 40$  impurities, 960 outer impurities, and a configuration average over 50 samples. The Fermi energy is obtained through

$$\int_{-\infty}^{E_F} D(E) dE = \frac{M \times LS}{\Omega} a_H^{*3}, \quad (15)$$

at 0 K. Of course,  $E_F$  was assumed to be the same in the whole sample, that is, in each of the LS configurations. This should be checked with the assumption made in the HFR calculations, namely, that the first  $M$  states of low energy were occupied in each configuration. When this

condition is not satisfied, we expect an internal charge transfer between different configurations, and the HFR calculations would have to be performed accordingly. This "charge inhomogeneity" generation can, in some aspects, be compared to the self-compensation effects in an early work.<sup>39</sup>

Performing the calculation, the IDS are obtained, as shown in Fig. 15 for the impurity concentration  $p = 0.5$  (corresponding to  $9.6 \times 10^{17} \text{cm}^{-3}$  for Si:P).

In order to obtain a microscopic view of the IDS, we have used the inverse participation ratio (IPR) that is also a measure of localization of the eigenstates.<sup>34,35,38</sup> It is defined as

$$(\text{IPR})_{i\sigma} = \left[ \sum_{j=1}^M |B_{ji\sigma}|^4 \right] / \left[ \sum_{j=1}^M |B_{ji\sigma}|^2 \right]^2, \quad (16)$$

for the  $i$ th eigenstate with  $\sigma$ -spin, where  $B_{ji\sigma}$  comes from Eq. (9). The IPR, dots appearing on Fig. 15, varies from 1, corresponding to a state which is as localized as possible, to  $1/M$ , corresponding to a state which is as extended as possible. Here, we are faced with the combined effects of diagonal and off-diagonal disorder, in contrast to the case of only the off-diagonal disorder. With decreasing impurity concentration, that combined effect helps states to become localized. This agrees with the assertion of Yonezawa<sup>40</sup> in her calculation in a two-dimensional square lattice. There, the diagonal and off-diagonal matrix elements of the sites are characterized respectively by different uniform distributions, where the degree of disorder is considered, instead of concentration.

For low concentration, most of the states have an IPR between 0.5 and 1.0 indicating an isolated impurity state or a pair state. Going to intermediate regions approaching  $N_c$ , where large clusters become more probable than isolated close pairs, the IPR for case (b) delocalizes less rapidly than for case (a), indicating a shift in the energy of the

delocalized conducting states. Even for such higher concentrations, some of the occupied states will be localized, which is supported by the absorption measurements on doped silicon by Schmid,<sup>41</sup> who also theoretically estimated the band-gap narrowing, using arguments rather similar to the work of Berggren and Sernelius,<sup>18</sup> and the calculation on direct-gap GaAs by Serre et al.,<sup>42</sup> who focused attention on the relative multiple-impurity scattering and impurity-concentration fluctuation, obtaining a band tailing. In a recent paper of Sernelius,<sup>18</sup> where the ion potentials are approximated by pure Coulomb potentials and the donor electrons are treated as an electron liquid surrounding the impurity ions, the high-stress optical birefringence and piezoresistance were investigated in heavily doped many-valley germanium. This calculation is carried out including the number of valleys ( $\nu = 4$ ), the effective mass, and a screening constant, and it shows that the band-tailing effects are reduced when the many-valley character of the HCB is taken into account. Now, taking the mean value of the IPR for each sample of the cluster, at a fixed concentration, and also the configuration average of the IPR ( $\langle \text{IPR} \rangle$ ) over all the sample clusters as shown in Fig. 16, Curve 3D (Curve 2D will be discussed later), we can see that in case (a); no valley effect, the  $\langle \text{IPR} \rangle$  for  $p < 0.3$  (corresponding to  $N < 5.76 \times 10^{17} \text{cm}^{-3}$  for Si:P), is greater than 0.5, while for case (b), with valley effect, only for  $p < 0.8$  ( $N < 1.92 \times 10^{18} \text{cm}^{-3}$ ) the  $\langle \text{IPR} \rangle$  is greater than 0.5. Calculating the magnetic susceptibility by a modified pair approximation including many-valley effects Andres et al.<sup>19</sup> showed that their results agree well with the experimental data up to concentration around  $1.2 \times 10^{18} \text{cm}^{-3}$  ( $p = 0.6$ ) for P-doped Si, which shows that the system is composed by isolated impurities or pairs of impurities. Our results, outlined above, are also in agreement with the conclusions reached by Thomas et al.<sup>19</sup> through their analysis of optical data.<sup>43</sup> Some experimental clues also exist in ESR (Ref. 44) investigation supporting this clustering evidence. For low concentration ( $N \leq 7.0 \times 10^{17} \text{cm}^{-3}$ ,  $p \leq 0.4$ ), hyperfine-split ESR lines exist and they are characteristic of electrons bound on donor sites. With increasing impurity concentration until clusters of eight or ten atoms form, this multiple line pattern fades into that of a single unresolved ESR line. For Si:P the delocalization occurs at

$N \approx 3.7 \times 10^{18} \text{ cm}^{-3}$  ( $p \approx 2.0$ ). It is worth noting that for the same spatial disorder, the electronic correlation is much affected by the many-valley effect. The overlap, the exchange, and the electron-hopping energy integrals on two neighboring donors are much reduced on the average and so is the broadening of the IDS, showing a new feature in the overall impurity states of indirect-gap semiconductors.

An example of a two-dimensional analogue of the IDS has been detected in the inversion layer of a metal-oxide-semiconductor field effect transistor (MOSFET). A good description of the structure and properties of these devices are given by Stern and Howard<sup>45</sup> and Ando et al.<sup>45</sup> The structure of such a device is that it consists of three layers: a metal electrode, an oxide layer, and the bulk semiconductor. If we consider a device where the semiconductor is p type, then it has the property that a n type inversion layer is produced at the interface with the oxide layer. It occurs as a result of the energy bands in the bulk semiconductor, near the interface, being bent down so that the bottom of the conduction band lies below  $\epsilon_F$ . This arises as a consequence of the presence of positive charges near the surface of the oxide layer, which are associated with impurity ions or other Coulomb centres, or through the application of an electric field normal to the surface. In this way the inversion layer becomes populated with electrons, and because they are in a deep potential well their motion is quantized normal to the surface, so that motion in the inversion layer is essentially two dimensional (2D). Because of the random field produced by the charge centres near the surface of the oxide layer, it is to be expected that the states near the bottom of the first electric subband will be localized. These devices have therefore received considerable attention experimentally and theoretically. Recently we have directed our attention for such studies in order to know better the behavior of the impurity states in a 2D system. A 2D HFR calculation was performed and the results for the  $\langle \text{IPR} \rangle$  is shown in Fig. 16. There we can see, compared to the  $\langle \text{IPR} \rangle$  calculation in 3D, how localized are the states in a 2D system. Also, results are shown for a one-band simulation formalism in Ref. 46. An extensive study of the 2D IDS, in the wake of Ref. 45, was done by da Cunha Lima et al.<sup>47,48,49</sup> Such

study will continue to pay very much our attention in order to have a real picture of the impurity states in 3D and 2D systems.

REFERENCES

- <sup>1</sup> P.W. Anderson, Phys. Rev. 109, 1492 (1958).
- <sup>2</sup> N.F. Mott, Metal-Insulator Transition (Taylor and Francis, London, 1974).
- <sup>3</sup> N.F. Mott, Philos. Mag. 26, 1015 (1972); Adv. Phys. 21, 785 (1972).
- <sup>4</sup> T.F. Rosenbaum, K. Andres, G.A. Thomas, R.N. Bhatt, Phys. Rev. Lett. 45, 1723 (1980); G.A. Thomas, M. Paalanan and T.F. Rosenbaum, Phys. Rev. B27, 3897 (1983).
- <sup>5</sup> D.J. Thouless, J. Phys. C8, 1803 (1975); Phys. Rev. Lett. 39, 1167 (1979).
- <sup>6</sup> P.P. Edwards and M.J. Sienko, Phys. Rev. B17, 2575 (1978).
- <sup>7</sup> J. Hubbard, Proc. A. Soc. London 281, 401 (1964).
- <sup>8</sup> A. Ferreira da Silva, R. Kishore and I.C. da Cunha Lima, Phys. Rev. B23, 4035 (1981).
- <sup>9</sup> The Metal-Insulator Transition in Disordered Systems, edited by L.R. Friedman and D.P. Tunstall (Scottish Universities Summer School in Physics, Edinburg, 1978).
- <sup>10</sup> M. Taniguchi and S. Narita, Solid St. Commun. 20, 131 (1976); S. Narita and M. Kobayashi, Philos. Mag. B42, 895 (1980).
- <sup>11</sup> H. Kamimura in Ref. 9.
- <sup>12</sup> In parts the introductory outline follows rather closely, Ref. 2, K.-F. Berggren (private report) and B.T. Debney (Internal Report - University of Birmingham).
- <sup>13</sup> K.-F. Berggren, Philos. Mag. 27, 1027 (1973); 30, 1 (1974); F. Martino, G. Lindel and K.-F. Berggren, Phys. Rev. B8, 6030 (1973).
- <sup>14</sup> K.-F. Berggren, J. Phys. C15, L45 (1982).
- <sup>15</sup> H. Kamimura, in Modern Problems in Condensed Matter Sciences, edited by M. Pollack and A.L. Efros, (North-Holland, Amsterdam, in press).

- <sup>16</sup> P.R. Cullis and J.R. Marko, Phys. Rev. B1, 632 (1970).
- <sup>17</sup> K. Jain, S. Lai, and M.V. Klein, Phys. Rev. B13, 5448 (1976).
- <sup>18</sup> K.-F. Berggren and B.E. Sernelius, Phys. Rev. B24, 1971 (1981);  
B.E. Sernelius, Phys. Rev. B27, 6234 (1983).
- <sup>19</sup> G.A. Thomas, M. Capizzi, F. De Rosa, R.N. Bhatt, and T.M. Rice, Phys.  
Rev. B23, 5472 (1981); K. Andres, R.N. Bhatt, P. Goalwin, T.M.  
Rice and R.E. Walstedt, Phys. Rev. B24, 244 (1981).
- <sup>20</sup> N.-I. Franzén and K.-F. Berggren, Philos. Mag. B23, 29 (1981); Phys.  
Rev. B25, 1993 (1982); N.-I. Franzén, Philos. Mag. B97, 565 (1983).
- <sup>21</sup> A. Ferreira da Silva and M. Fabbri (this issue) and references cited.
- <sup>22</sup> A. Ferreira da Silva, R. Riklund and K.A. Chao, Prog. Theor. Phys.  
62, 584 (1979); K.A. Chao, R. Riklund and A. Ferreira da Silva,  
Phys. Rev. B21, 5745 (1980); K.A. Chao, A. Ferreira da Silva and  
R. Riklund, Suppl. Prog. Theor. Phys. 72, 181 (1982).
- <sup>23</sup> T. Matsubara and Y. Toyozawa, Prog. Theor. Phys. 26, 739 (1961).
- <sup>24</sup> Y. Ishida and F. Yonezawa, Prog. Theor. Phys. 49, 731 (1973);  
N. Majlis, Proc. Phys. Soc. 90, 811 (1967); M. Weissmann and  
N.V. Cohen, J. Phys. F7, 913 (1977); B. Movaghan and G.W. Sauer,  
J. Phys. F9, 867 (1979).
- <sup>25</sup> A. Ferreira da Silva, I.C. da Cunha Lima and M. Fabbri, Phys. Letters  
A83, 463 (1981); Phys. Stat. Solidi (b) 115, 311 (1983).
- <sup>26</sup> K.A. Chao, A. Ferreira da Silva, J. Phys. C11, 3661 (1978); Int.  
J. Quantum Chem. 12, 461 (1978); Phys. Stat. Solidi (b) 90, K153  
(1978); Phys. Rev. B19, 4125 (1979).
- <sup>27</sup> A. Ferreira da Silva, J. Phys. C13, L427 (1980).
- <sup>28</sup> A. Ferreira da Silva, R. Micnas, I.C. da Cunha Lima and R. Kishore,  
Phys. Stat. Solidi (b) 120, K101 (1983).
- <sup>29</sup> T. Saso (preprints, reprints and private communication).
- <sup>30</sup> M. Kikuchi, J. Phys. Soc. Japan 25, 989 (1968).
- <sup>31</sup> H. Fritzsche in Ref. 9.

- <sup>32</sup> K. Nagasaka and S. Narita, *Solid. St. Commun.* 7, 467 (1969);  
F. Sugawara, T. Nakamura, H. Hirose and S. Kobayashi, Japan,  
*J. Appl. Phys.* 10, 1108 (1971).
- <sup>33</sup> W. Kohn and J.M. Luttinger, *Phys. Rev.* 98, 915 (1955); W. Kohn, in  
*Solid State Physics*, edited by F. Seitz and D. Turnbull (Academic,  
New York, 1957), Vol. 5.
- <sup>34</sup> M. Fabbri and A. Ferreira da Silva, *Phys. Rev.* B29, 5764 (1984).
- <sup>35</sup> M. Fabbri and A. Ferreira da Silva, *J. Non-Crystalline Solids* 55,  
103 (1983).
- <sup>36</sup> F. Yonezawa, Y. Ishida and F. Martino, *J. Phys.* F6, 1091 (1976);  
N. Majlis and E. Anda, *J. Phys.* C11, 1607 (1978); L.F. Perondi,  
A. Ferreira da Silva and M. Fabbri, (this issue).
- <sup>37</sup> The author acknowledges Dr. Rolf Riklund for discussions about this  
scheme.
- <sup>38</sup> R. Riklund and K.A. Chao, *Phys. Rev.* B26, 2168 (1982).
- <sup>39</sup> R.N. Bhatt and T.M. Rice, *Philos. Mag.* B42, 859 (1980); *Phys. Rev.*  
B23, 1920 (1981).
- <sup>40</sup> F. Yonezawa, *J. Non-Crystalline* 35-36, 29 (1980).
- <sup>41</sup> P.E. Schmid, *Phys. Rev.* B23, 5531 (1981).
- <sup>42</sup> J. Serre, A. Ghazali, and P. Leroux Hugon, *Phys. Rev.* 23, 1971  
(1981).
- <sup>43</sup> See also K.-F. Berggren in this issue.
- <sup>44</sup> D.F. Holcomb in Ref. 9 and references cited.
- <sup>45</sup> F. Stern and W.E. Howard, *Phys. Rev.* 163, 816 (1967); T. Ando,  
A.B. Fowler and F. Stern, *Rev. Mod. Phys.* 54, 437 (1982); F.  
Stern (this issue).
- <sup>46</sup> I.C. da Cunha Lima, A. Ferreira da Silva and M. Fabbri, *Surface  
Science* 134, 135 (1983).
- <sup>47</sup> I.C. da Cunha Lima and A. Ferreira da Silva, *Phys. Rev.* B30, 4819  
(1984).

<sup>48</sup> I.C. da Cunha Lima, A. Ferreira da Silva, P.S. Guimarães, L.F. Perondi and J.R. Senna, Phys. Rev. B (1985) (in press).

<sup>49</sup> I.C. da Cunha Lima (this issue).

FIGURE CAPTIONS

- Fig. 1- Bandstructures of a crystalline material and the corresponding density of states (below). Shaded regions denote occupied states.  $\epsilon_F$  denotes the Fermi energy. See text.
- Fig. 2- Density of states of a disordered system.  $\epsilon_c$  denotes the mobility edge. See text.
- Fig. 3- Overlap of two impurity Hubbard ( $D^0$  and  $D^-$ ) subbands.  $\epsilon_1$ ,  $\epsilon_2$  and  $\epsilon_3$  indicate the activation energies involved in the system (Ref. 9)
- Fig. 4- The diagonal and off-diagonal matrix elements  $V_{ij}$  and  $V_{ij}$ , respectively for MT, AMO and HL schemes, as functions of the inter-impurity distance  $R_{ij}$ .
- Fig. 5- Impurity density states (IDS) for various values of the dimensionless impurity concentrations  $P=32\pi N a_H^{*3}$ .  $N$  is the true impurity concentration and  $a_H^*(\alpha^{-1})$  is the Bohr radius of the impurity. The position of  $E_F$  is indicated by dot-dashed lines, and the bottom of the HCB by dotted line (AMO scheme).  $V_0=2E_I$ , and  $E_I$  is the ionization energy.
- Fig. 6- Dimensionless conductivity  $L$  as function of  $E_F$  for different values of compensation  $K$  and concentration  $P$ . The dots on the curves represent the degrees of compensation  $K$ . The dashed line indicates  $h$  for  $K=0$ .
- Fig. 7- Hubbard IDS for various values of  $P$ . The position of  $E_F$  is indicated by dashed lines and the bottom of the HCB by a dotted line.
- Fig. 8- Hubbard IDS for various values of  $P$ . The arrows indicate the  $E_F$  and the dot-dashed lines refer to the bottom of the HCB. (a) The dashed lines refer to the case of neglecting the many-valley character of the HCB. The full lines refer to the inclusion of the latter assumption, i.e., for Ge:Sb. (b) IDS for Si:P.

Fig. 9- Variation of the energy gap,  $\Delta g$ , between the IDS, compared to the experimental activation energy,  $\epsilon_2$ , of Ge:Sb, for different concentration.

Fig. 10- Variation of  $\Delta g$  between the IDS, compared to the observed  $\epsilon_2$  of Si:P, with concentration.

Fig. 11- The overlap and electron hopping energy integrals as a function of distance  $R$  between impurity centres. The dashed and full-drawn wiggly curves refer to the anisotropic cases. The dashed and full smooth curves refer to the case of neglecting the oscillatory factor deriving from the many-valley character of the HCB. The latter case is relevant to, for example, n-type CdS. The vector,  $\vec{R}$ , is between the two impurity centres in the  $\langle 100 \rangle$  direction. The arrows indicate the mean separation of donors at different concentrations. The effective Bohr radius used was  $a_H^* = 17.2 \text{ \AA}$ . The impurity critical concentration for MNM transition in Si:P is  $3.74 \times 10^{18} \text{ cm}^{-3}$ .

Fig. 12- IDS without [(a) and (b)] and with [(c) and (d)] many-valley character of the Si-HCB. The nonorthogonality effect is presented in (b) and (d). The HCB is set at zero energy. The arrow indicates the  $E_F$ . The dots correspond to the inverse participation ratio. 200 configurations of 50 impurities, each for  $P=1.0$ , were used.

Fig. 13- Variation of  $\langle D^- \rangle$  and  $\langle D^0 \rangle$  as a function of  $\alpha$ .  $N=3.8 \times 10^{16} \text{ cm}^{-3}$

Fig. 14- IDS for different values of  $\alpha$ .  $P=0.0125 \equiv N=2.3 \times 10^{16} \text{ cm}^{-3}$

Fig. 15- IDS without (a) and with (b) many-valley character of the Si HCB. The HCB is set at zero energy. Shaded area represents the overlap of split bands. The dots correspond to the IPR, and  $p=0.5$  corresponds to  $9.6 \times 10^{17} \text{ cm}^{-3}$ , for Si:P. The arrow indicates  $E_F$ .

Fig. 16-  $\langle L_{n\sigma} \rangle \equiv \langle IPR \rangle$  for various values of impurity concentration  $P(2D)$  and  $P'(3D)$ . For comparison  $P'=1.0$  ( $N^{1/3}a_H^*=0.21$ , Mott's relation) corresponds to  $N=1.9 \times 10^{18} \text{cm}^{-3}$ ,  $P=16$  ( $N^{1/3}a_H^*=0.28$ ) corresponds to  $2.66 \times 10^{12} \text{cm}^{-2}$ . The dots represent the individual  $L_{n\sigma}$ , in 2D case, for each configuration, at a fixed  $P$ .

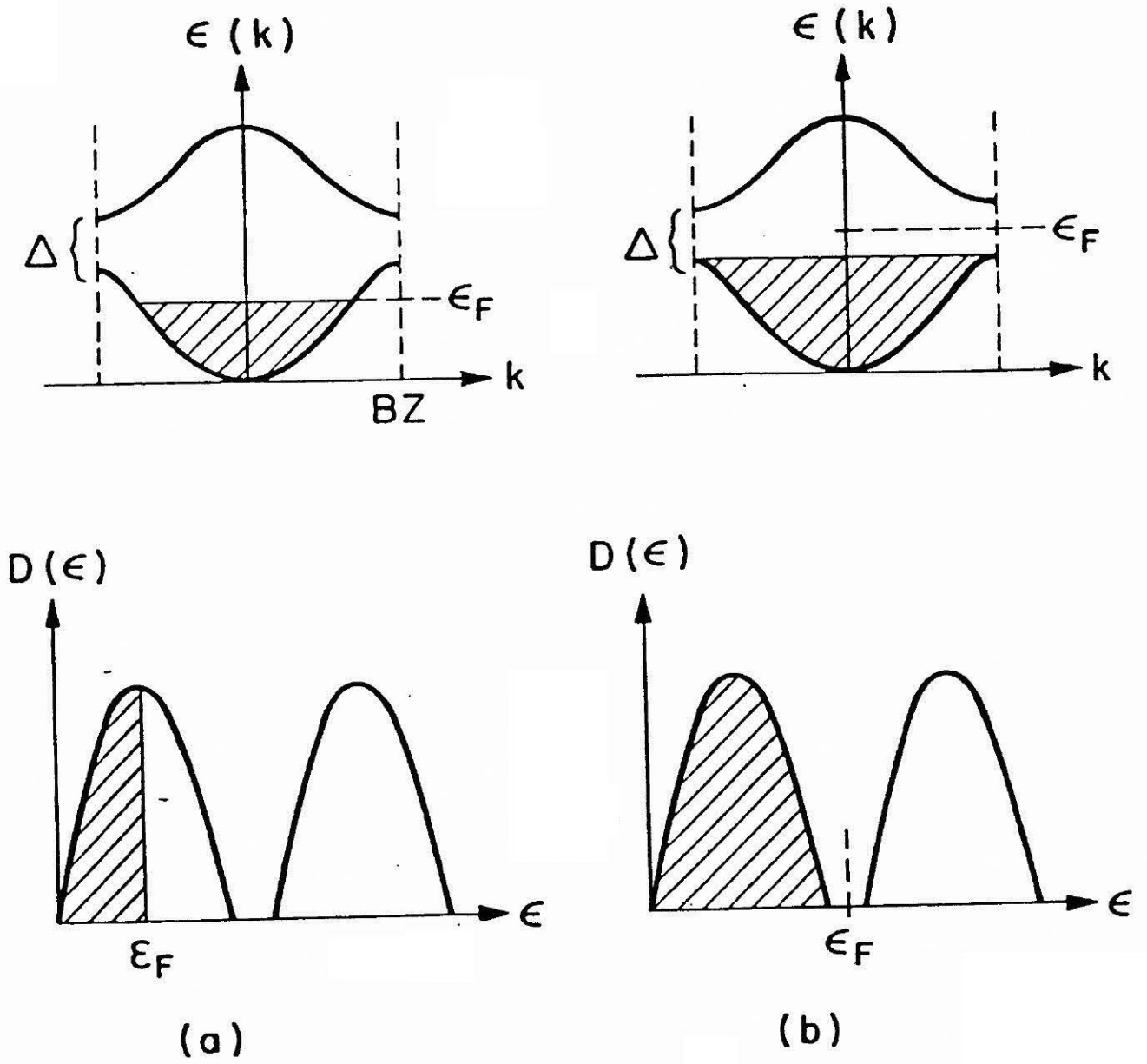


Fig. 1 - A. Ferreira da Silva

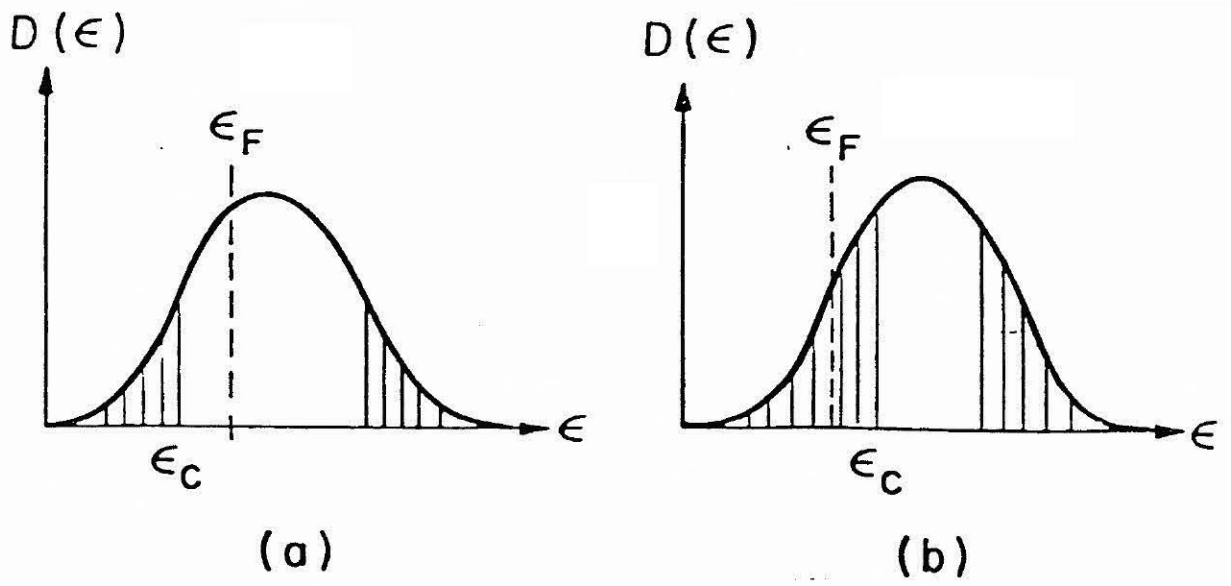


Fig. 2 - A. Ferreira da Silva

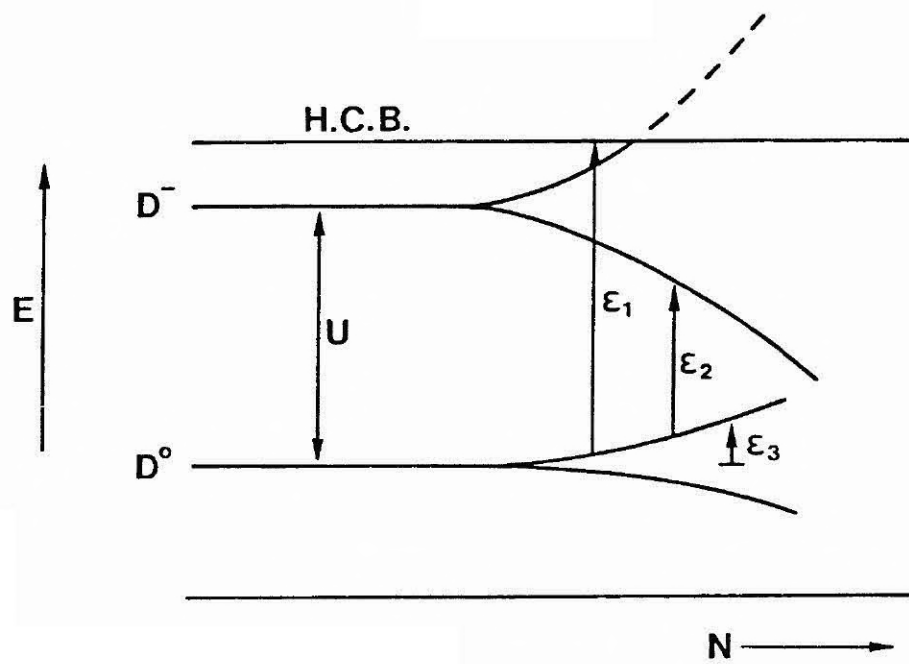


Fig. 3 - A. Ferreira da Silva

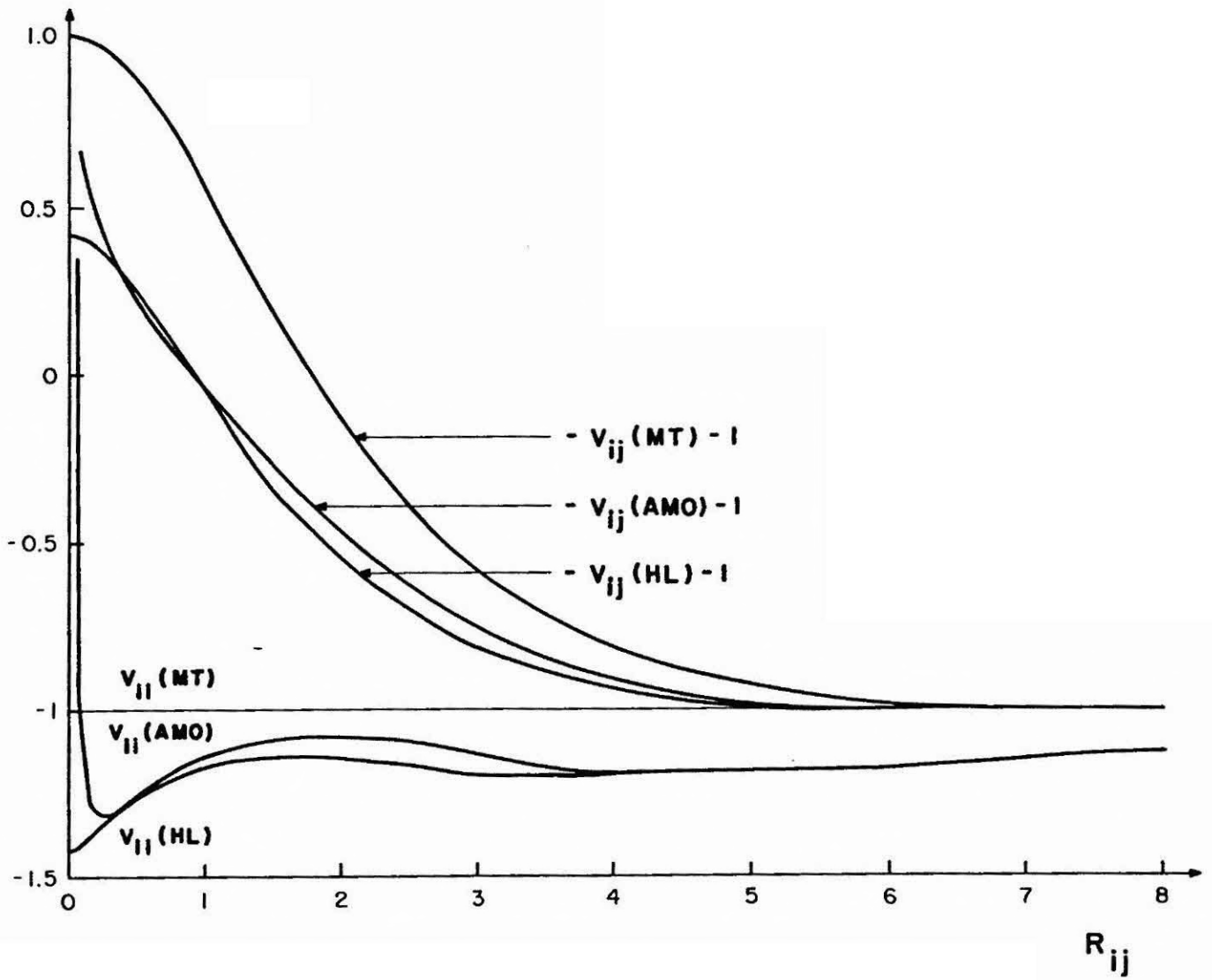


Fig. 4 - A. Ferreira da Silva

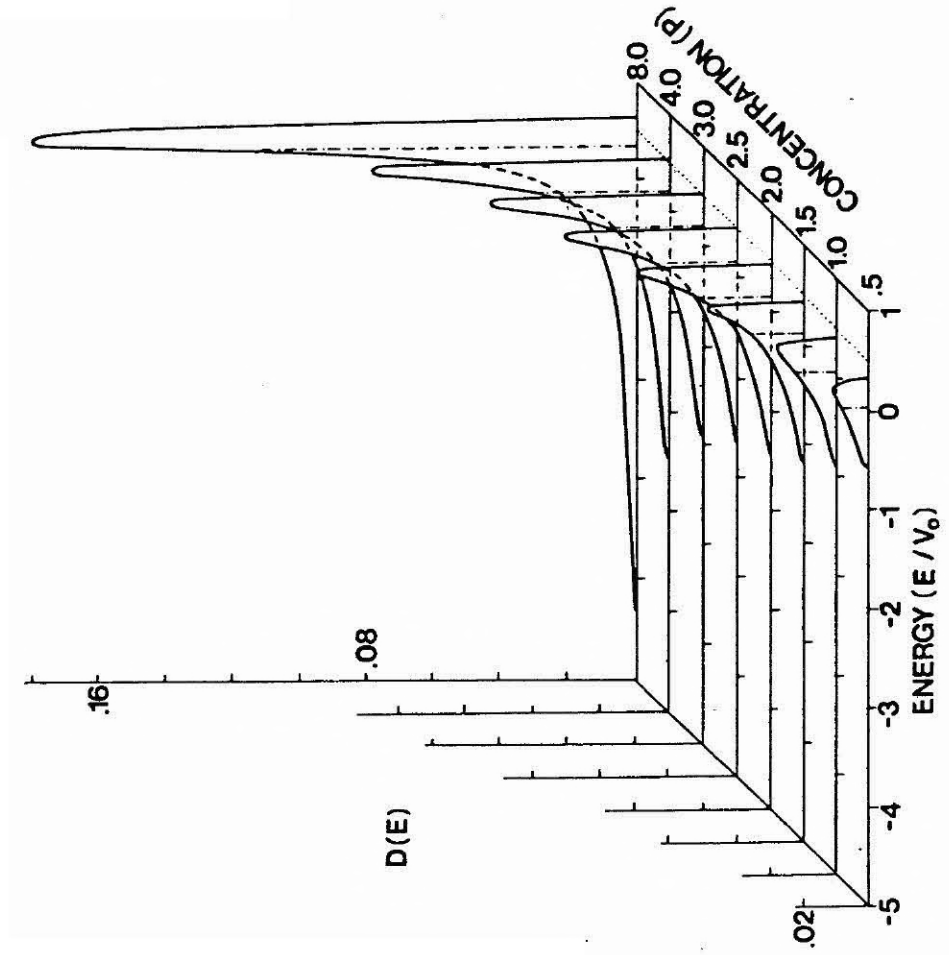


Fig. 5 - A. Ferreira da Silva

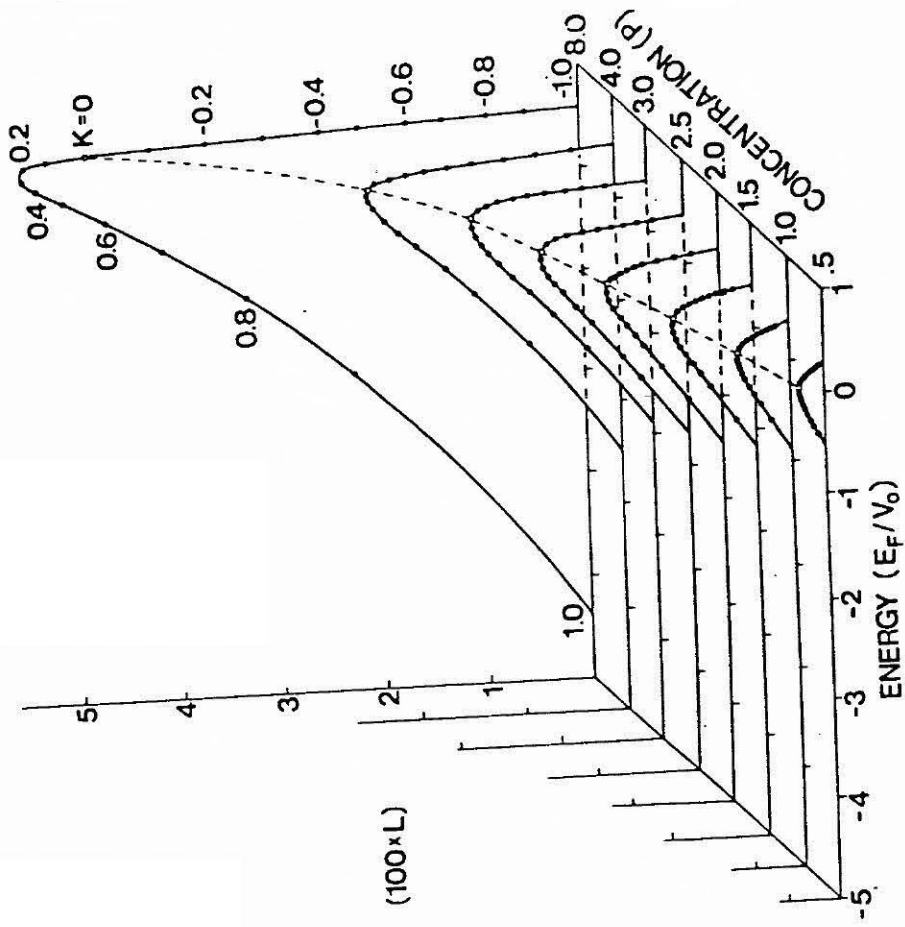


Fig. 6 - A. Ferreira da Silva

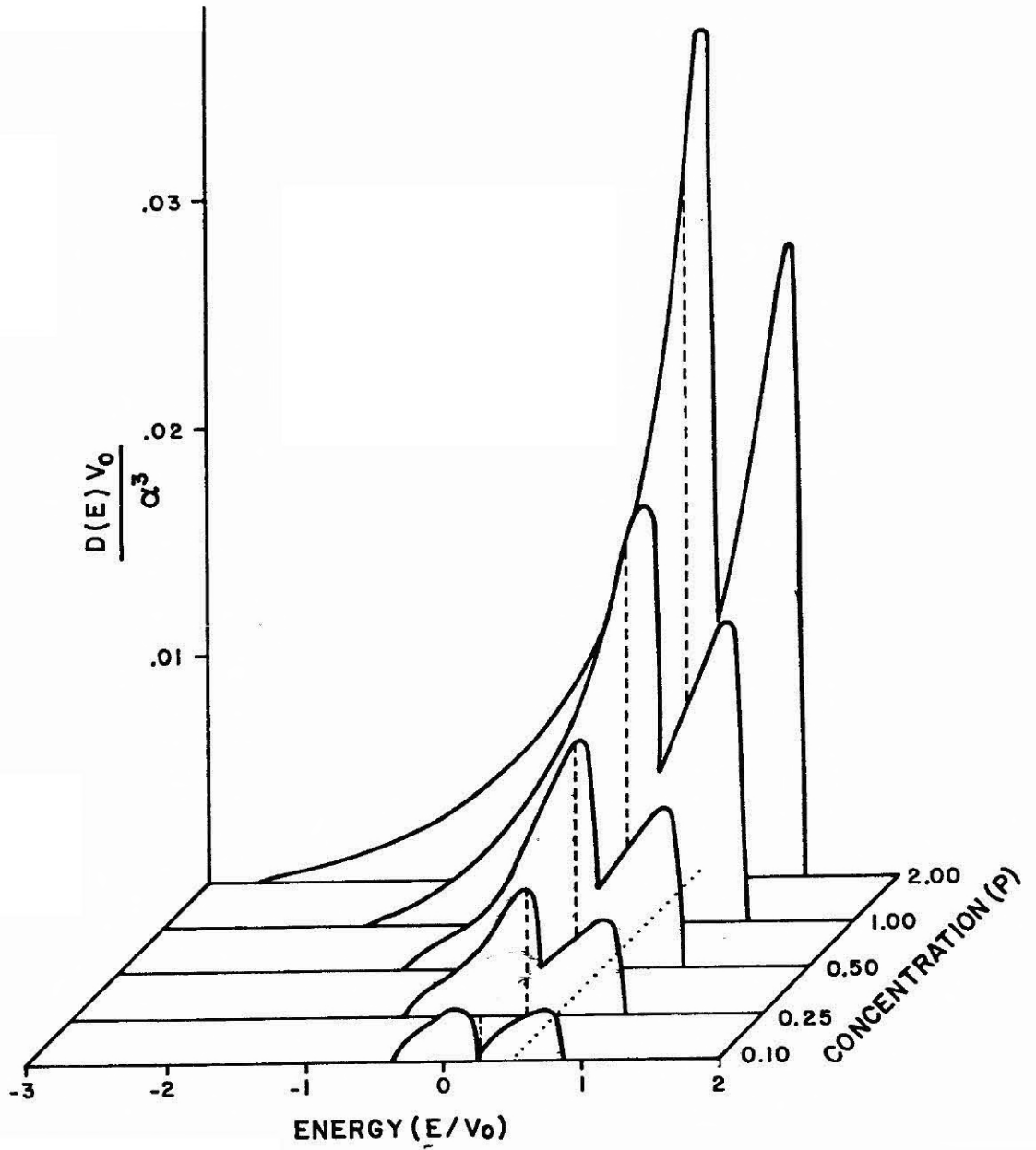


Fig. 7 - A. Ferreira da Silva

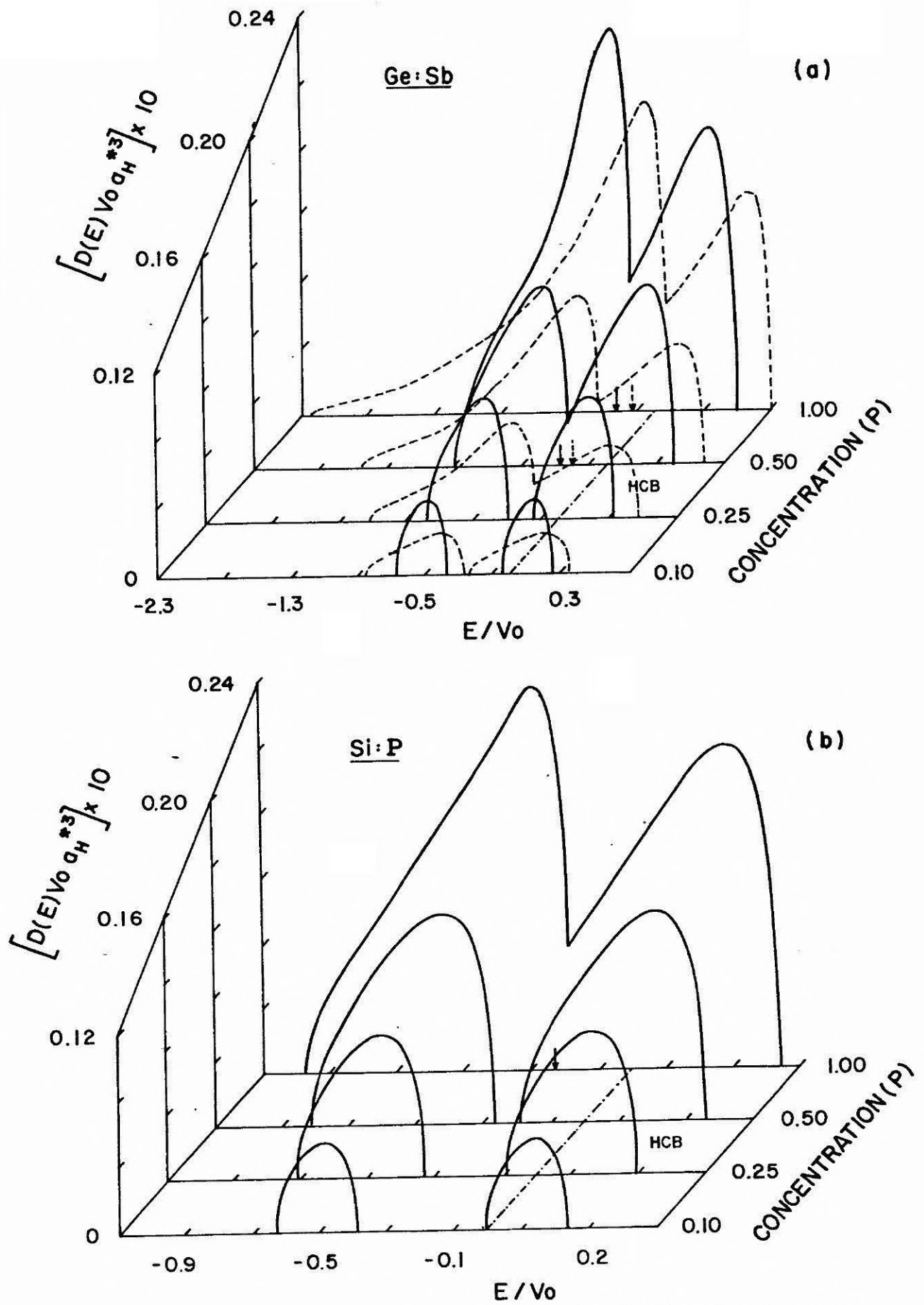


Fig. 8 - A. Ferreira da Silva

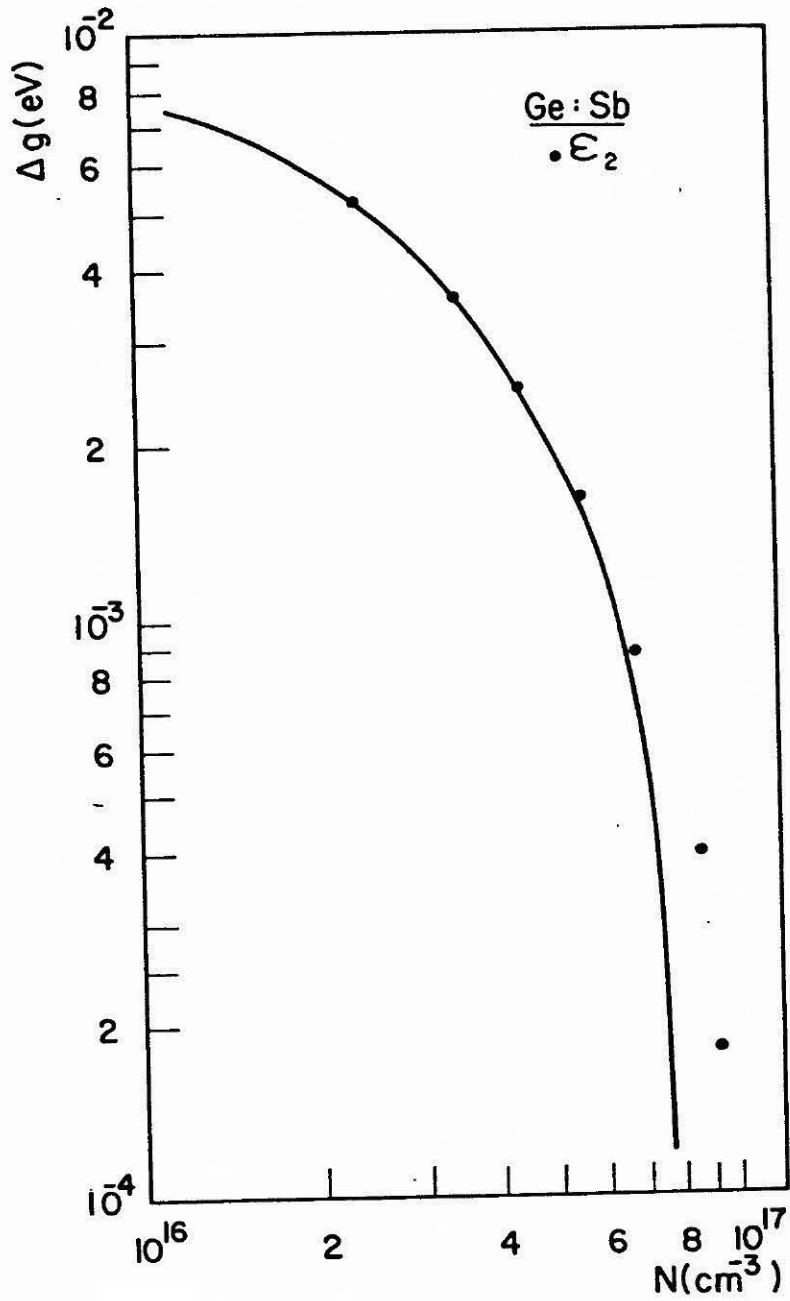


Fig. 9 - A. Ferreira da Silva

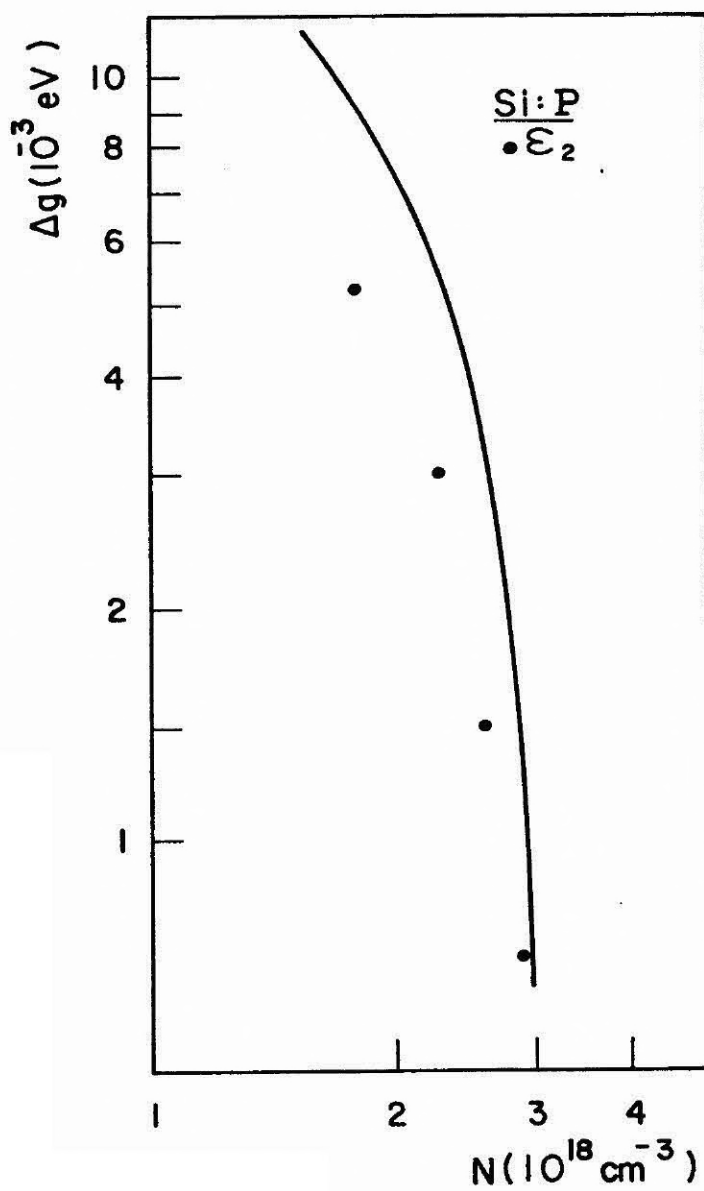


Fig. 10 - A. Ferreira da Silva

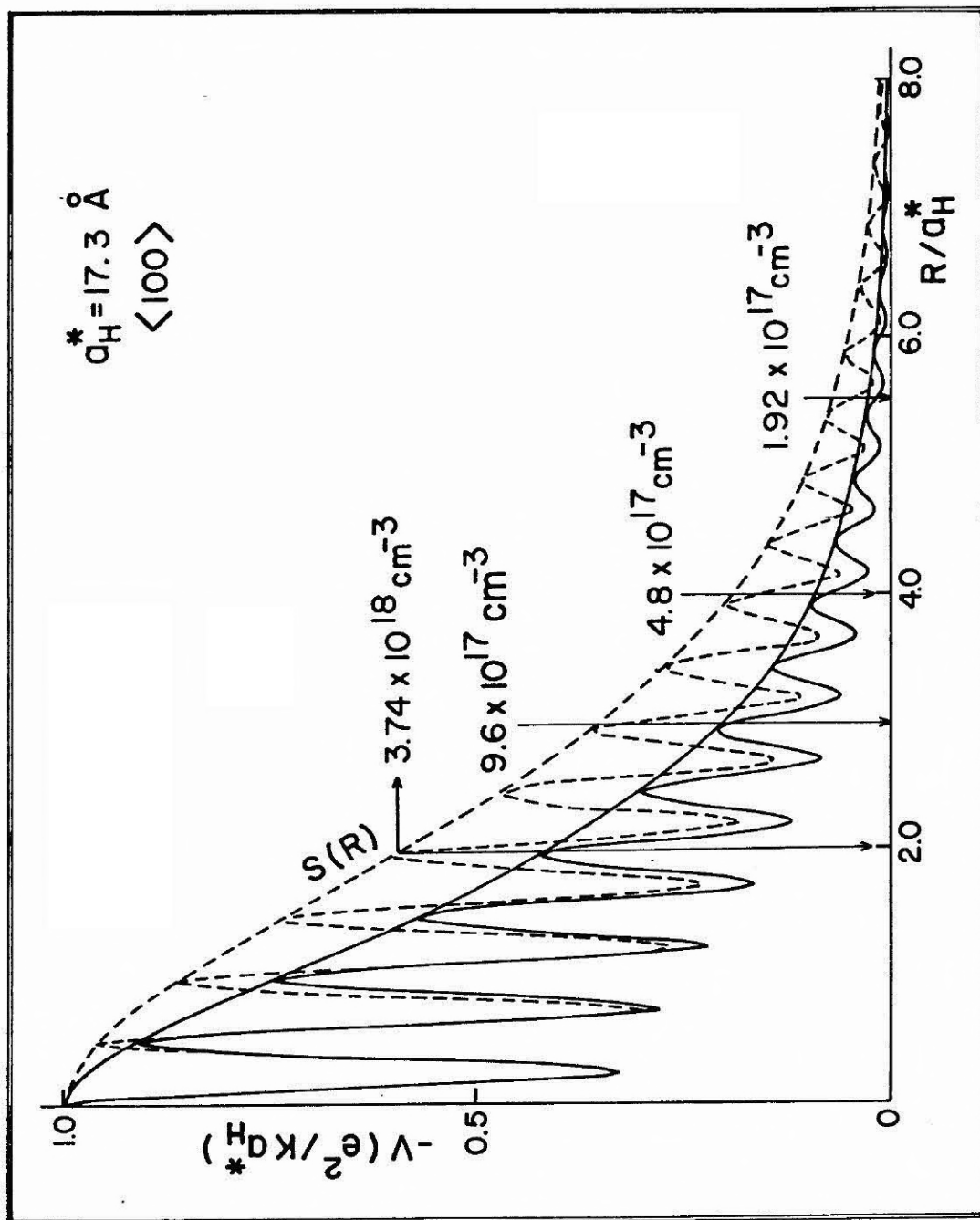


Fig. 11 - A. Ferreira da Silva

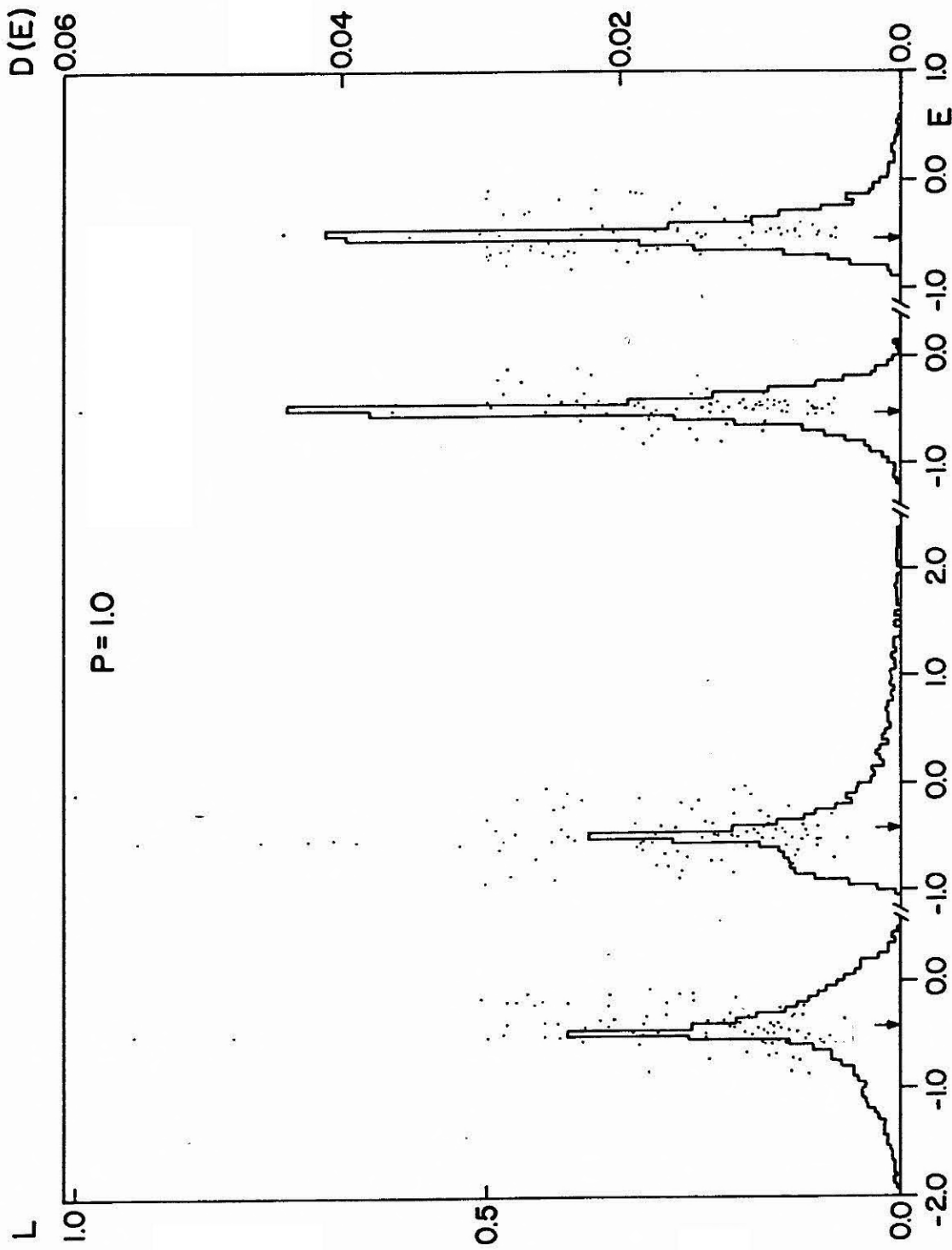


Fig. 12 - A. Ferreira da Silva

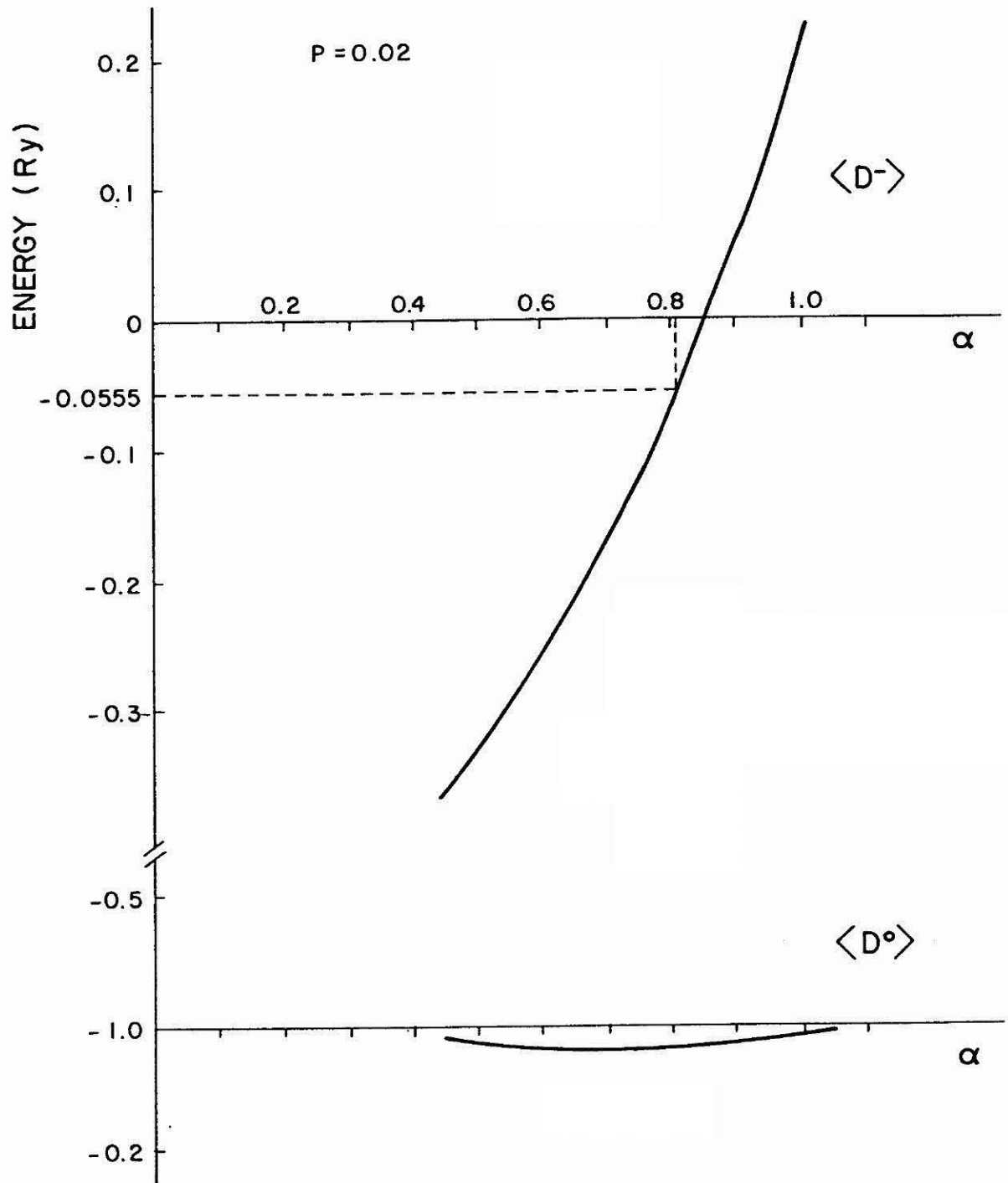


Fig. 13 - A. Ferreira da Silva

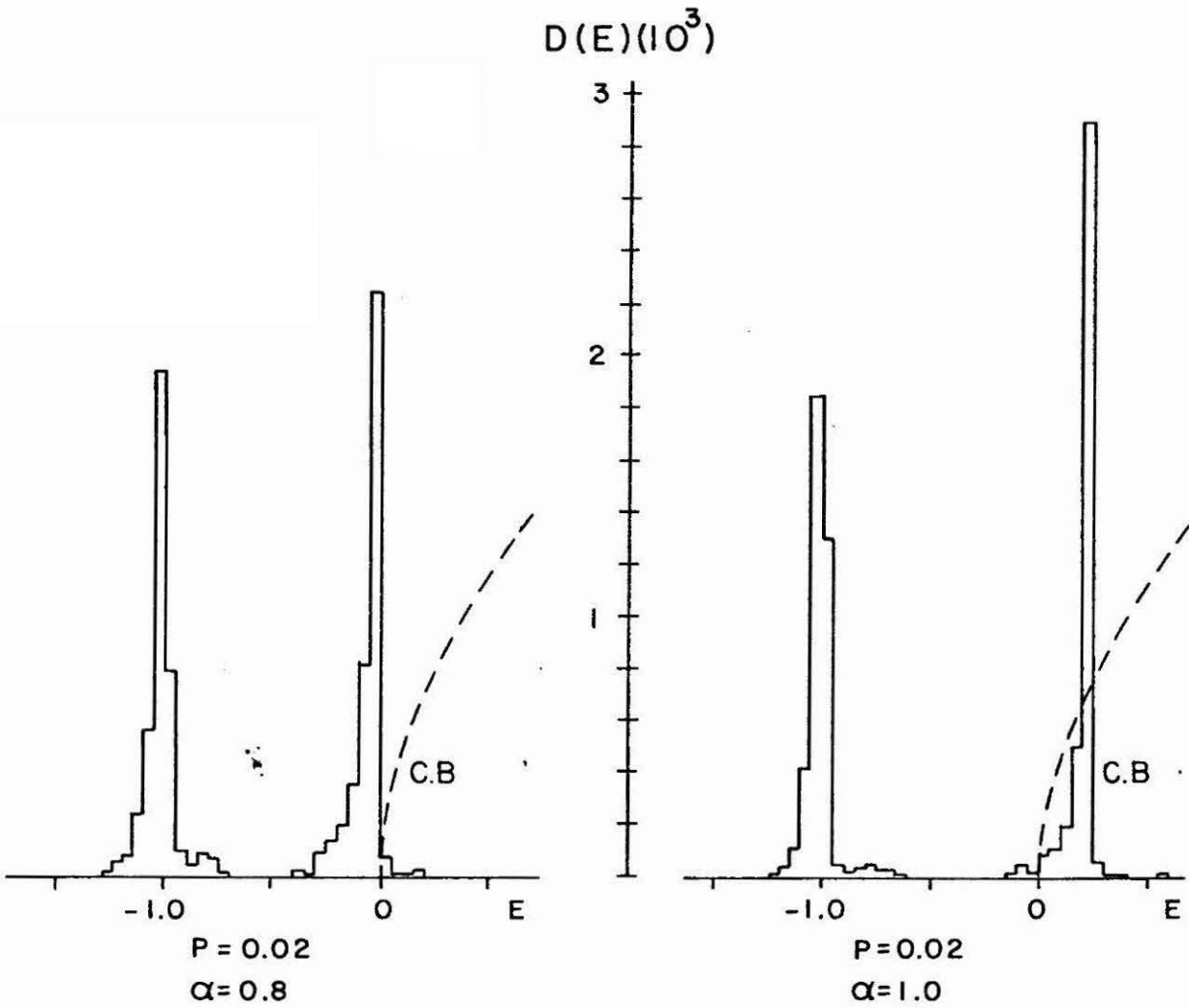
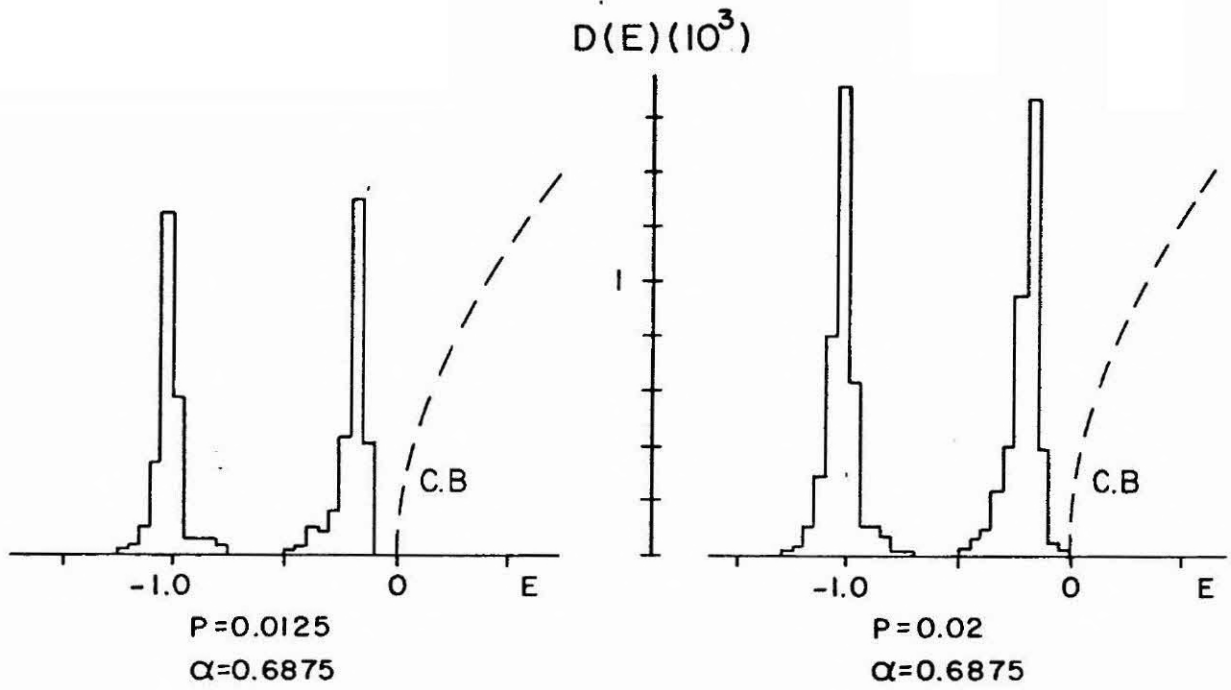


Fig. 14 - A. Ferreira da Silva

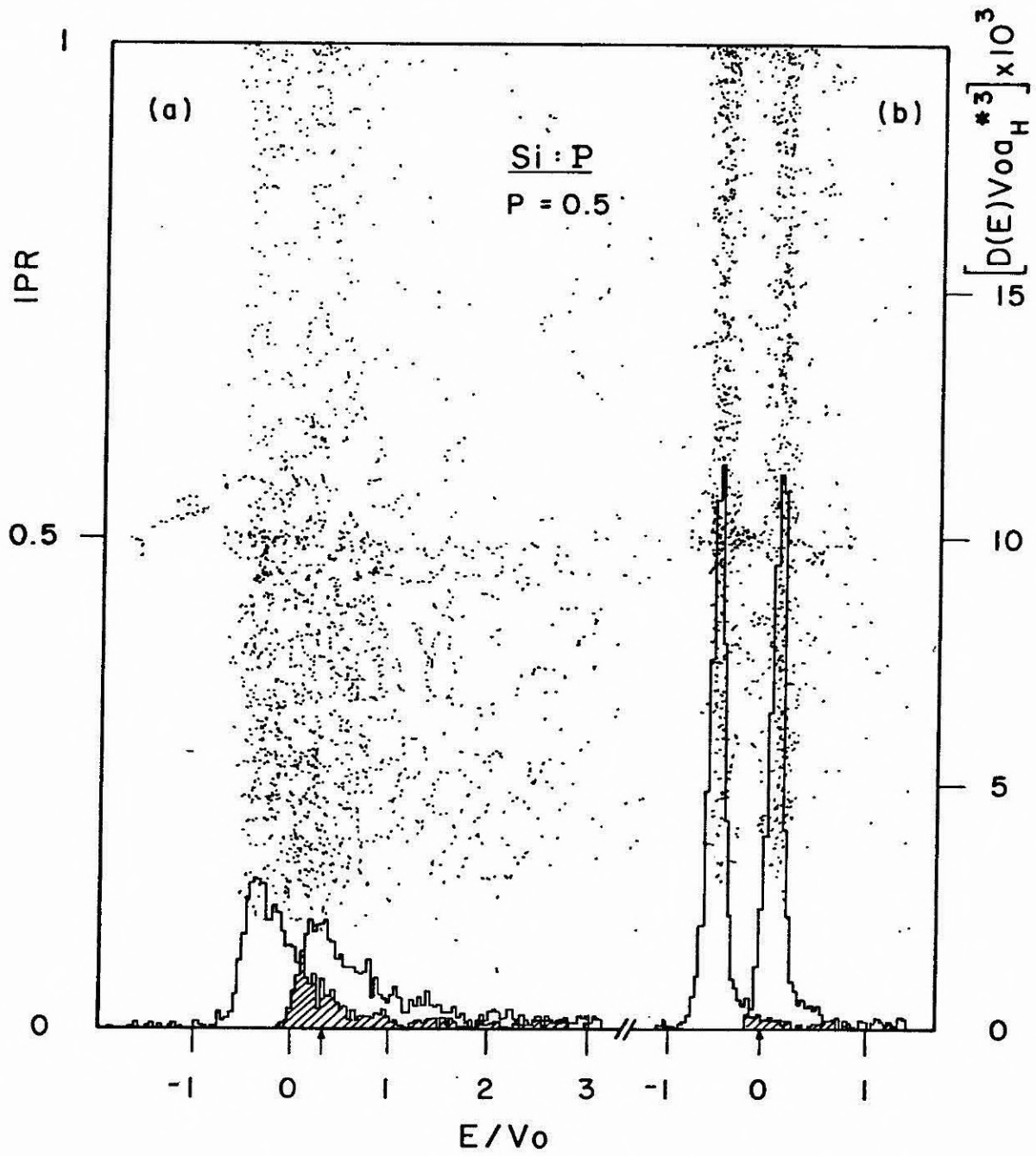


Fig. 15 - A. Ferreira da Silva

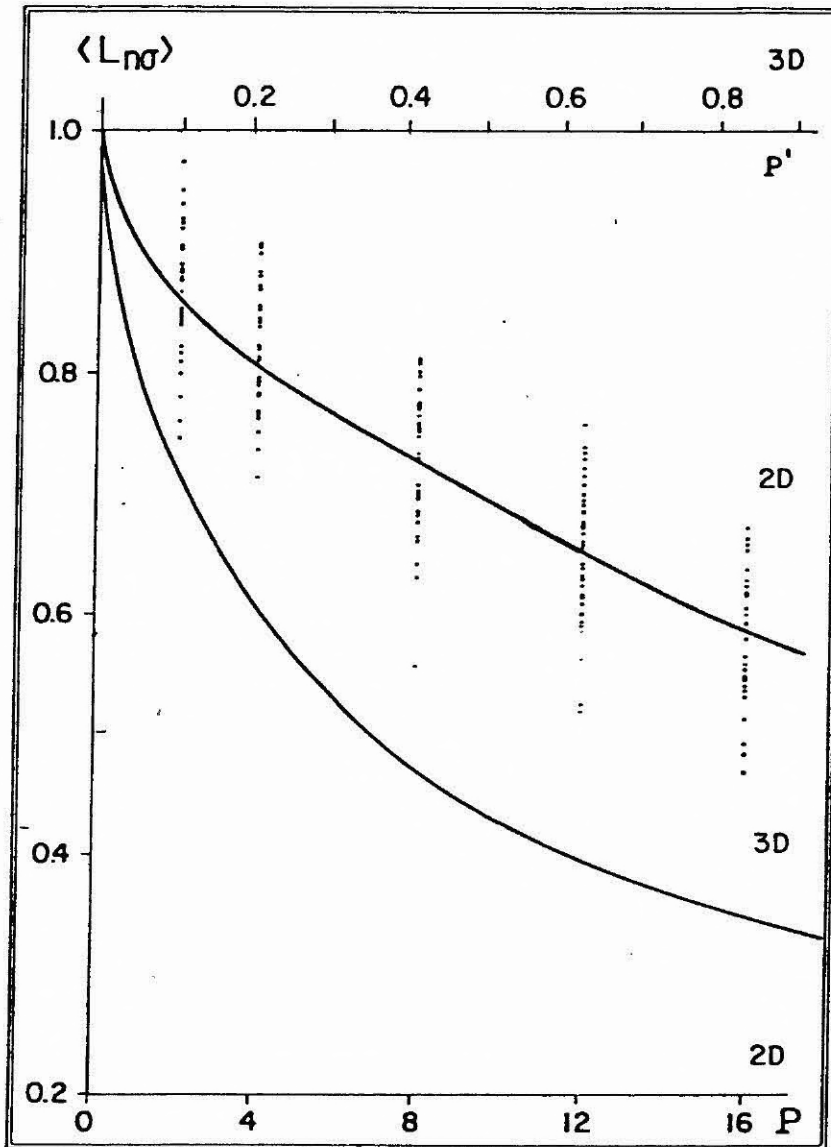


Fig. 16 - A. Ferreira da Silva